Magnetic Resonance Imaging 59 (2019) 68–76

Contents lists available at ScienceDirect

Magnetic Resonance Imaging

journal homepage: www.elsevier.com/locate/mri

Original contribution

Magnetic resonance elastography of the brain: A study of feasibility and reproducibility using an ergonomic pillow-like passive driver

Xunan Huang[a], Hatim Chafi[b], Kenneth L. Matthews II[b], Owen Carmichael[c], Tanping Li[d], Qiguang Miao[a], Shuzhen Wang[a,*], Guang Jia[a,*]

[a] School of Computer Science and Technology, Xidian University, Xi'an, Shaanxi, 710071, China
[b] Department of Physics and Astronomy, Louisiana State University, Baton Rouge, LA 70803, USA
[c] Pennington Biomedical Research Center, Baton Rouge, LA 70808, USA
[d] School of Physics and Optoelectronic Engineering, Xidian University, Xi'an, Shaanxi 710071, China

ARTICLE INFO

Keywords:
Magnetic resonance elastography
Human brain
Ergonomic passive driver
Frequency
Reproducibility

ABSTRACT

Magnetic resonance elastography (MRE) can be used to noninvasively resolve the displacement pattern of induced mechanical waves propagating in tissue. The goal of this study is to establish an ergonomically flexible passive-driver design for brain MRE, to evaluate the reproducibility of MRE tissue-stiffness measurements, and to investigate the relationship between tissue-stiffness measurements and driver frequencies.

An ergonomically flexible passive pillow-like driver was designed to induce mechanical waves in the brain. Two-dimensional finite-element simulation was used to evaluate mechanical wave propagation patterns in brain tissues. MRE scans were performed on 10 healthy volunteers at mechanical frequencies of 60, 50, and 40 Hz. An axial mid-brain slice was acquired using an echo-planar imaging sequence to map the displacement pattern with the motion-encoding gradient along the through-plane (z) direction. All subjects were scanned and rescanned within 1 h. The Wilcoxon signed-rank test was used to test for differences between white matter and gray matter shear-stiffness values. One-way analysis of variance (ANOVA) was used to test for differences between shear-stiffness measurements made at different frequencies. Scan-rescan reproducibility was evaluated by calculating the within-subject coefficient of variation (CV) for each subject.

The finite-element simulation showed that a pillow-like passive driver is capable of efficient shear-wave propagation through brain tissue. No subjects complained about discomfort during MRE acquisitions using the ergonomically designed driver. The white-matter elastic modulus (mean ± standard deviation) across all subjects was 3.85 ± 0.12 kPa, 3.78 ± 0.15 kPa, and 3.36 ± 0.11 kPa at frequencies of 60, 50, and 40 Hz, respectively. The gray-matter elastic modulus across all subjects was 3.33 ± 0.14 kPa, 2.82 ± 0.16 kPa, and 2.24 ± 0.14 kPa at frequencies of 60, 50, and 40 Hz, respectively. The Wilcoxon signed-rank test confirmed that the shear stiffness was significantly higher in white matter than gray matter at all three frequencies. The ranges of within-subject coefficients of variation for white matter, gray matter, and whole-brain shear-stiffness measurements for the three frequencies were 1.8–3.5% (60 Hz), 4.7–6.0% (50 Hz), and 3.7–4.1% (40 Hz).

An ergonomic pneumatic pillow-like driver is feasible for highly reproducible in vivo evaluation of brain-tissue shear stiffness. Brain-tissue shear-stiffness values were frequency-dependent, thus emphasizing the importance of standardizing MRE acquisition protocols in multi-center studies.

1. Introduction

Palpation has been used to diagnose many diseases in the breast, prostate, liver, and other organs that are accompanied by changes in the viscoelastic properties of soft tissues [1]. However, palpation is subjective and does not provide quantitative information. In addition, the brain is surrounded by a hard skull and therefore is ineligible for palpation. Clinical imaging modalities, such as computed tomography (CT) and magnetic resonance imaging (MRI), which can be used to assess brain tissue morphology and anatomy, do not provide

Abbreviations: MRE, magnetic resonance elastography; MRI, magnetic resonance imaging; ANOVA, analysis of variance; CV, coefficient of variation; ROIs, regions of interest

* Corresponding authors.
E-mail addresses: shuzhenwang@xidian.edu.cn (S. Wang), gjia@xidian.edu.cn (G. Jia).

https://doi.org/10.1016/j.mri.2019.03.009
Received 26 October 2018; Received in revised form 8 March 2019; Accepted 8 March 2019

information about viscoelastic properties the way palpation does [2]. Ultrasound elastography (UTE) has shown promise in quantifying such mechanical properties, but it is rarely used to quantify brain-tissue stiffness due to the limited acoustic window associated with the presence of the skull [3].

Magnetic resonance elastography (MRE) is a quantitative imaging technology that allows for the noninvasive measurement of the mechanical properties of soft tissues. MRE combines magnetic resonance imaging (MRI) with mechanical wave propagation and uses motion-sensitive magnetic-field gradients to record the harmonic displacements of soft tissue in MRI phase images, which are used to estimate tissue viscoelasticity [4]. MRE requires the use of a mechanical device—a *driver*—that is applied to the organ under study and generates shear waves during the MRI scan. Shear waves enter the tissue or organ and displace the tissue while motion-sensitive magnetic resonance displacement imaging is performed. The displacements are used to estimate the elasticity (or stiffness) of the tissue, using mathematical models of tissue properties [5,6]. This technique has been used to evaluate the mechanical properties of the liver [7], brain [8,9], breast [10,11], and prostate [12]. Such MRE measurements have been validated against intraoperative surgical assessments [13].

The stiffness of brain tissue is of great clinical interest because it may be modified by several diseases, such as dementia [14,15], hydrocephalus [16,17], brain tumors [13], multiple sclerosis [18,19], and neuroinflammatory diseases [20]. Tissue stiffness is also of interest in the study of normal brain development [21]. However, the optimal design of the MRE driver for brain applications is not clear. Commercially available drivers are largely designed for liver applications, and thus are not flexible enough to conform to the contour of the head. Nor are liver drivers small enough to fit inside the typical head coil. Alternative driver designs, including head cradles, bite bars, and flexible pillows, have been designed for brain MRE. Pattison et al. proposed a pneumatic actuator in the feline brain model [22]. Yeung et al. designed a driver for the head and neck, which was used to measure the elastic modulus of the parotid gland, lymph nodes, and thyroid gland [23]. Latta et al. designed a paired system that includes an active driver and a passive driver that must both be used together, which occupies a large volume of space [24]. Hiscox et al. evaluated a head pillow with a large expansion area covering the upper part, the lower part and the left and right parts of the head. Air was transferred to the head pillow through two tubes [6]. A rectangular pillow-shaped passive driver designed by Murphy et al. was placed at the bottom of the head coil during MRE scanning [14,25].

The purpose of this study was to develop a comfortable and MR-head-coil-compatible passive driver for use with a commercially available MRE system (Resoundant, Inc.) and evaluate its performance on healthy volunteers. Referring to the design structure of Huston et al. [26], we designed a head pillow that is simple to use and easy to connect to a commercially available active-driver system. During MRE scans, it is placed below the head in contact with the head(Fig. 1A). We used two-dimensional (2D) finite-element simulation to evaluate shear-wave propagation in the brain with a passive occipital actuator of this design. We then conducted experiments to investigate differences between gray- and white-matter stiffness at different driver frequencies (60 Hz, 50 Hz, and 40 Hz). We hypothesized that white- and gray-matter shear-stiffness measurements made with MRE using this flexible ergonomic driver design would be reproducible and have a within-subject coefficient of variation below 15% at each driving frequency.

2. Materials and methods

2.1. Subjects

This study protocol was approved by the institutional review board of Pennington Biomedical Research Center (PBRC). Ten healthy volunteers with a median age of 28 years (range: 24–38 years) were recruited for MRE scanning of the brain. They included 6 males and 4 females (mean weight: 77.2 kg; range: 48.7–94.4 kg). All subjects provided written informed consent and underwent two identical MRE examinations separated by a one-hour interval. The criteria for inclusion were that the subjects must be between the ages of 18 and 50 years, have no metal fragments in the body, be free of metallic tattoos, and not be pregnant.

2.2. MRE ergonomic passive driver

The following factors were considered in the head-MRE passive acoustic driver design: (1) The passive driver must be in contact with the head and have sufficient ergonomic performance to guarantee the comfort of the MRE-scanned subject. (2) MRI-compatible materials should be selected to ensure the driver can be placed inside the MRI scanner. (3) The driver should be designed to have appropriate dimensions to fit into an MRI head coil. (4) The passive driver should have a solid, flexible structure while ensuring that it can be smoothly filled with air in the initial deflated state.

The adjustable air-filter material was selected to act as the solid, flexible structure so that the driver would not be crushed by the weight of the head before being inflated. The air filter (3 M, St. Paul, MN) is made from fiberglass and has a thickness of 2.5 cm. It was cut to have a circular diameter of 15.2 cm. A polyvinyl chloride (PVC) tube with an inside diameter of 1.3 cm was placed in contact with the air filter. Two circular cutouts made of a supple PVC fabric (Gaiam, Louisville, CO) were used to cover the air filter (Fig. 1B). The cutouts were stitched tightly together to cover the air filter and the PVC tube. The edges of the cutouts were also glued together to minimize air leakage during the MRE scan. An MRI skin marker (Beekley Medical, Bristol, CT) was placed on the center of the driver to guarantee that the driver would be placed in the imaging area of interest. Fig. 1C shows the internal structure of the pillow-like driver.

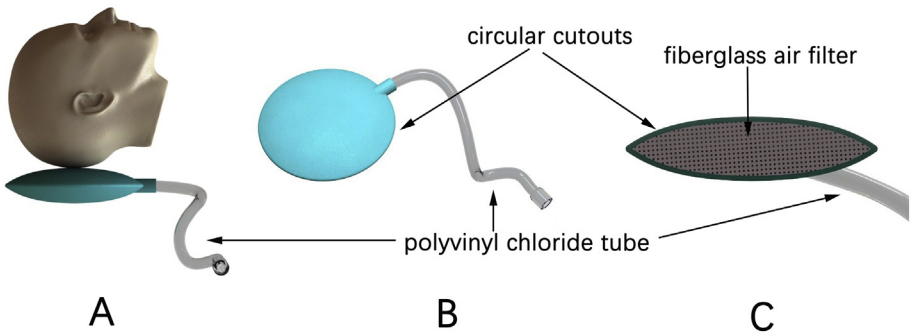

Fig. 1. The flexible ergonomic driver designed for MRE brain scans. A flexible reducer was used to connect it to a rigid PVC tube with an inside diameter of 1.9 cm, which was fed through a conduit and terminated at the active driver in the equipment room.

2.3. Two-dimensional (2D) finite-element simulation

An axial brain slice was designed including bone (shear-wave velocity Cs = 1.47 × 105 cm/s), air (Cs = 0 cm/s), gray matter (Cs = 182 cm/s), white matter (Cs = 197 cm/s), and CSF (Cs = 0 cm/s). In the simulation, the air-gap region was neglected and treated as the bone region. Free boundary condition was used in this simulation. CSF was treated as fluid, which cannot support shear wave. Shear wave was considered as propagating only in the bone and gray- and white-matter regions. A Gmsh code was used to mesh the 2D brain slice into quadrilaterals, with an average element size of 2 mm in the bone region and 1 mm in the white- and gray-matter regions [27]. In order to understand the real-time shear-wave propagation in the 2D brain slice, the brain was treated as an isotropic elastic medium. A 2D simulation used the spectral element method code specfem2d [28] for the shear wave perpendicular to the 2D brain slice (SV).

2.4. MRI examination

An ergonomic passive driver was connected via a 7.3-m tube to an excitation driver that was placed in the MRI equipment room. The Resoundant active driver was placed outside the MRI unit in the equipment room. The active driver was connected to the MRI system via a British naval connector (BNC) cable and to a GE MR750W 3 .0T scanner via an Ethernet cable. The signal generator, located in the active driver, was triggered by and synchronized with the MRE pulse sequence.

The passive driver was placed on the bottom surface inside the head coil, with the subject's head resting on the driver. The subject was lying on the bed and the subject's head was scanned in a supine position. The MRE skin marker was centered in the area of interest on the localizer. This experiment was performed on a 3 .0T MR scanner (MR750W, GE Healthcare, Waukesha, WI). Axial T2-weighted images covering the entire brain were acquired using a spin-echo (SE) sequence (repetition time [TR]: 3000 ms; echo time [TE]: 94.4 ms; thickness: 10 mm; field of view: 240 mm; matrix size: 256 × 256; flip angle: 142°). A single-slice image containing the prefrontal lobe, temporal lobe, corpus callosum, and occipital lobe was chosen for examination. Eight time-phase amplitude and phase images were acquired using a 2D spine echo echo-planar imaging (EPI) MRE sequence (repetition time [TR]: 1000 ms; echo time [TE]: 62–84 ms; echo train length [ETL]: 64; thickness: 10 mm; field of view: 240 mm; matrix size: 64 × 64; flip angle: 90°), which was modified to include an additional motion-coding gradient in the through-plane (z) direction. The variability in TE stemmed from the change in frequency of the share wave; i.e., TE was 62.4 ms for 60 Hz, 70.8 ms for 50 Hz, and 83.3 ms for 40 Hz. The motion-encoding frequency was set to match the driver frequency. A pneumatic actuator synchronized with the pulse sequence was used to vibrate the brain at three mechanical frequencies: 60 Hz, 50 Hz, and 40 Hz. After the scans were completed, the subjects removed themselves from the table and then were reset on the table and rescanned using the same protocol. All subjects were scanned and rescanned within a one-hour interval. The acquisition time for each MRE scan was 8 s.

2.5. Image processing and analysis

The Helmholtz inversion [29] of the MRE data was performed using GE's post-processing software (GE MR Touch DV23.1). In order to verify the reliability of the data, the phase-difference SNR [30] (PDSNR, the product of phase amplitude and magnitude SNR) value was measured. The phase images were converted to a waveform image that showed the displacement of the tissue through the plane. The wave image was inverted again, and a grayscale elasticity map was generated.

The white-matter, gray-matter, and whole-brain regions of interest (ROIs) were plotted on T2-weighted images using ImageJ processing software (Version 1.49v, Bethesda, Maryland) (Fig. 2A). Two white-matter ROIs and two gray-matter ROIs were chosen. A brain ROI was drawn using a single donut-shaped ROI encompassing the whole brain. The ROIs were placed in areas where adequate wave propagation was clearly visible (Fig. 2B). The ROIs were pasted to the elasticity map to measure tissue stiffness. The grayscale elasticity map was imported into MATLAB (Version R2013a, Natick, Massachusetts) for the application of a jet color map and the application of color bars in kPa (Fig. 2C). The shear stiffness (μ) was measured in the white matter, the gray matter, and the whole brain from the scan and rescan data at frequencies of 60 Hz, 50 Hz, and 40 Hz.

2.6. Statistical analyses

We tested for significant statistical differences between the white- and gray-matter shear-stiffness measurements using the Wilcoxon signed-rank test. The comparison of the shear-stiffness measurements of all white and gray matter at all three frequencies was performed using the Wilcoxon signed-rank test.

For the gray-matter, white-matter, and whole-brain shear-stiffness measurements, the discrepancies among them at all three frequencies were assessed using one-way ANOVA. The sum of squares due to the source (SS), degrees of freedom (df), mean sum of squares due to the source (MS), found variation of group averages (F), and expected variations of group averages (F critical) were calculated for all three frequency groups in the white matter, gray matter, and whole brain region. A difference of $P < 0.05$ was considered significant.

We then assessed the reproducibility of our tissue-stiffness measurement using the within-subject coefficient of variation (CV) and through plotting with Bland-Altman plots. CV is calculated as the square root of the mean of the ratio of the squared difference of the scan and rescan measurements to the squared average of the scan and rescan measurements for all healthy volunteers:

$$\sqrt{\frac{1}{n}\sum_{i=1}^{n}\frac{(\mu_{s(i)}-\mu_{r(i)})^2}{\left(\frac{\mu_{s(i)}+\mu_{r(i)}}{2}\right)^2}}\times 100\%,$$

where μ_s is the first shear-stiffness scan measurement, μ_r is the repeated shear-stiffness measurement, and n is the number of subjects (n = 10). The within-subject CV was calculated for μ measurements for gray matter, white matter, and the whole brain.

3. Results

3.1. Shear-wave propagation pattern in the brain

There were a total of 8964 nodes and 8675 elements covering the bone, gray-, and white-matter regions in the 2D finite-element simulation. Fig. 3B provides a snapshot of shear-wave propagation. From the simulated wave propagation result, the shear wave propagates quickly along the bone region due to the high bone shear-wave velocity and then penetrates into the gray and white region. The simulation exhibits the process of efficient shear-wave propagation through brain tissue by using a pillow-like passive-driver system.

3.2. Shear modulus measurements

The phase-difference SNR map was calculated from a subject's eight time-phase amplitude and phase images at different driver frequencies (60 Hz, 50 Hz, and 40 Hz). The mean PDSNR value (mean ± standard deviation) for whole brain were 189 ± 109 (60 Hz), 525 ± 329 (50 Hz), and 1592 ± 741 (40 Hz). Usually SNR > 5 or 3 is adequate to estimate robust stiffness values [6,14,22,30,31]. These results indicate that the PDSNR value of phase images meets the threshold requirements to guarantee an accurate elastography reconstruction.

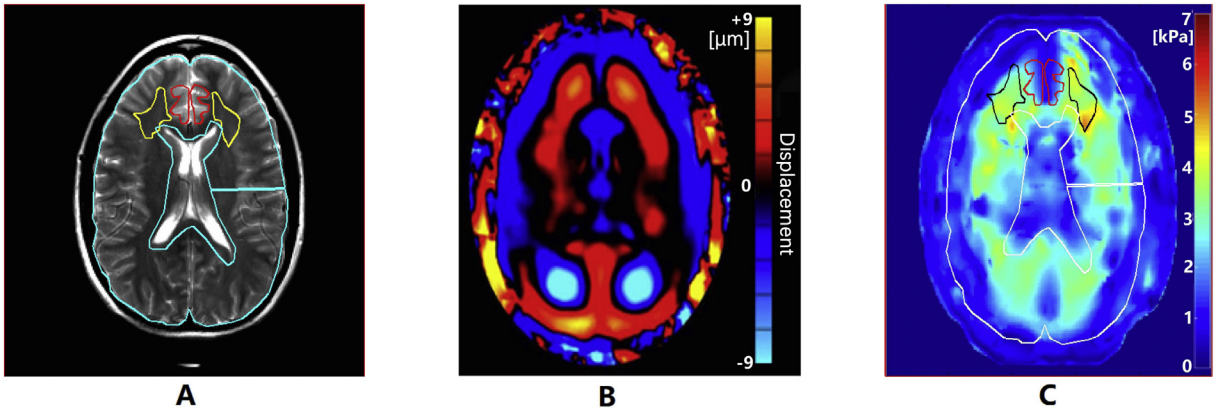

Fig. 2. A single T2-weighted image was used for anatomical reference for all three frequencies. The yellow, red, and blue ROIs encompass white matter, gray matter, and whole brain, respectively (A). The wave images show adequate shear-wave propagation (B). Elastograms were reconstructed with the Helmholtz inversion algorithm (C). White matter ROI included 441 voxels on T2-weighted image or 27 voxels on MRE image, with an area of 388 mm^2. Gray matter ROI included 716 voxels on T2-weighted image or 45 voxels on MRE image, with an area of 629 mm^2. Whole brain ROI included 17,140 voxels on T2-weighted image or 1072 voxels on MRE image, with an area of 15,065 mm^2. (For interpretation of the references to color in this figure legend, the reader is referred to the web version of this article.)

3.3. Shear modulus measurements

All 10 healthy volunteers underwent a head MRE examination with a newly designed pillow-like pneumatic driver, and no one complained about discomfort during either the initial scans or rescans. The validity of the driver design is verified theoretically by mechanical analysis. The MRE examination results showed that the shear waves generated by the pneumatic actuators were effectively transmitted into the brain tissue as a whole, as shown in Fig. 4.

At a driver frequency of 60 Hz, the shear stiffness of white-matter, gray-matter, and whole-brain ROIs ranged from 3.26 to 4.40 kPa, 2.61 to 4.16 kPa, and 3.13 to 3.56 kPa, respectively. At a driver frequency of 50 Hz, the white-matter shear stiffness ranged from 2.84 to 4.43 kPa, the shear stiffness of gray matter ranged from 2.25 to 3.30 kPa, and the whole-brain shear stiffness ranged from 2.90 to 3.26 kPa. At a driver frequency of 40 Hz, the white-matter shear stiffness ranged from 2.77 kPa to 3.79 kPa, the gray-matter shear stiffness ranged from 1.65 to 2.93 kPa, and the shear stiffness for the whole brain ranged from 2.38 to 2.80 kPa.

The box plot of Fig. 5 shows the full range variation of the shear stiffness of white matter and gray matter at 60, 50, and 40 Hz. The modulus measurements exhibited significant difference between white matter and gray matter at three frequencies with P values < 0.05. For white-matter, gray-matter, and whole-brain stiffness measurements, there was a power exponent of 0.333, 0.97, and 0.604 with r^2 values of 0.88, 0.998, and 0.977, respectively.

3.4. Shear stiffness at multiple frequencies

Table 1 shows the means and standard deviations of shear stiffness of white matter, gray matter, and whole brains for all subjects at all three frequencies (60 Hz, 50 Hz, and 40 Hz).

The following null hypothesis was tested through analysis of variance: The driver frequency has no effect on shear-stiffness measurements (H_0: $\mu_{60\ Hz} = \mu_{50\ Hz} = \mu_{40\ Hz}$.). Table 2 summarizes the ANOVA results for white matter, gray matter, and the whole brain. The changes in group mean (F) at different frequencies were found to be greater than the expected changes in white matter, gray matter, and the whole brain (F critical). This shows that we must reject the null hypothesis.

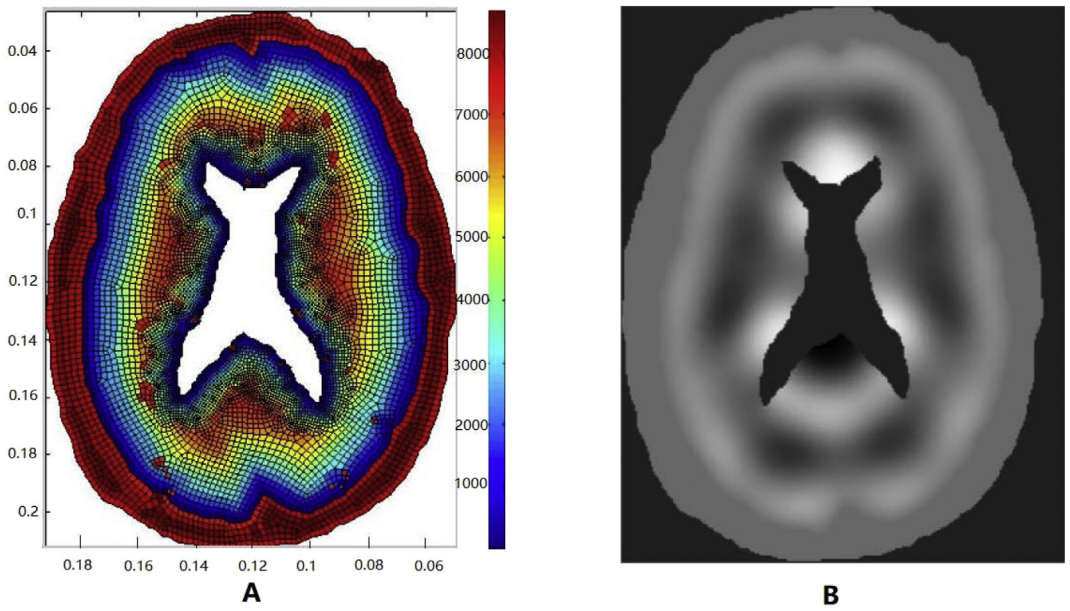

Fig. 3. Approximate mesh size for finite-element analysis: Bone region 2 mm; white- and gray-matter region 1 mm (A). A snapshot of shear-wave propagation (B).

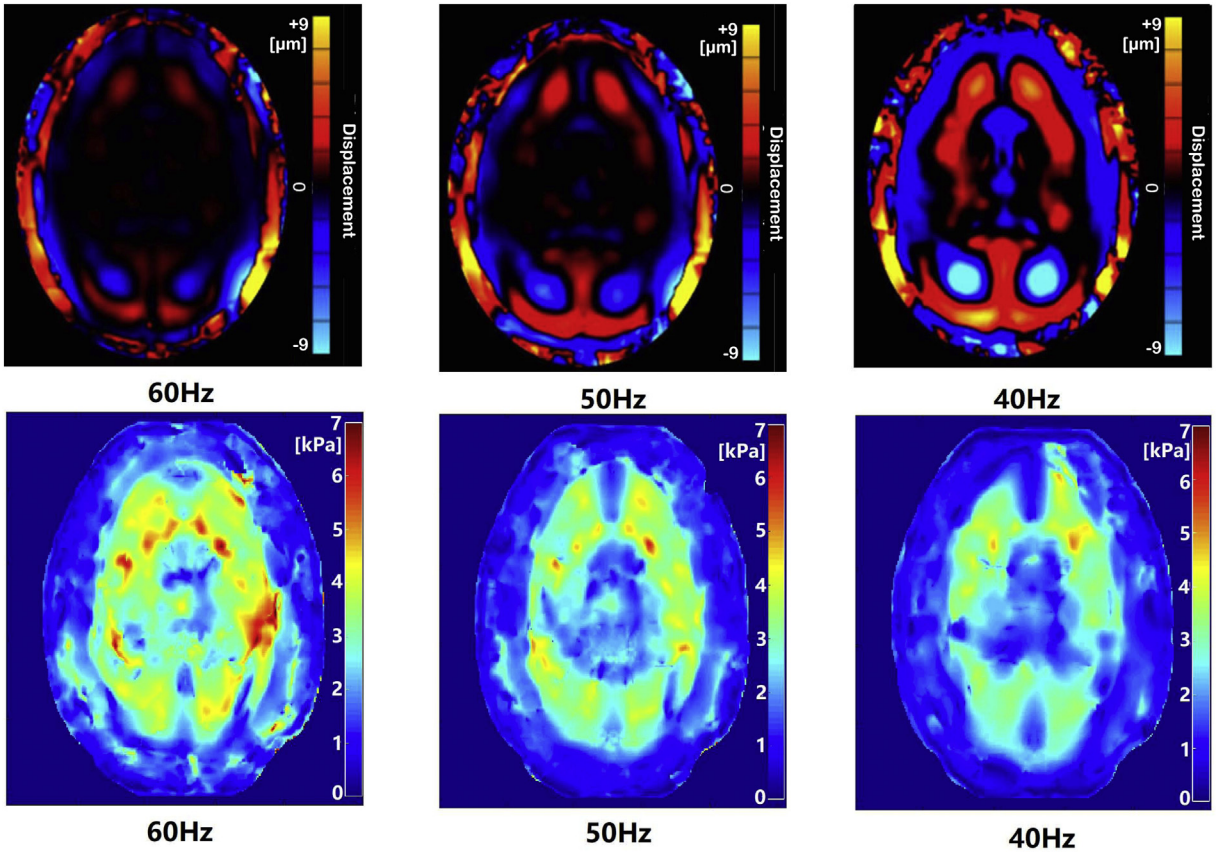

Fig. 4. Scan-wave images (upper row) and elastogram images (bottom row) for subject 2 at 60 Hz (left), 50 Hz (middle), and 40 Hz (right). (The central part of the brain tissue seems dark in the wave images at 50 and 60 Hz, however with signals strong enough for reconstruction and stiffness measurement.)

3.5. Scan-rescan reproducibility

Fig. 6 and supplemental materials show the Bland-Altman plot [32] of the difference between scan and rescan shear-stiffness measurements for all subjects at all three frequencies (60 Hz, 50 Hz, and 40 Hz). The mean differences between scans and rescans for white matter were 0.06 kPa (60 Hz), −0.02 kPa (50 Hz), and −0.05 kPa (40 Hz). The mean differences between scans and rescans for gray matter were 0.11 kPa (60 Hz), 0.15 kPa (50 Hz), and −0.02 kPa (40 Hz). The mean differences for the whole brain were 0.01 kPa (60 Hz), 0.08 kPa (50 Hz), and 0.01 kPa (40 Hz).

Fig. 7 lists the within-subject coefficients for drive frequencies of 60 Hz, 50 Hz, and 40 Hz. At 50 Hz, the within-subject coefficients of variance for white-matter, gray-matter, and whole-brain shear-stiffness measurements reached their respective maximum values of 4.1%, 6.0%, and 3.5%. At 40 Hz, the within-subject coefficients of variance for the whole-brain and gray-matter shear-stiffness measurements reached their respective minimum values of 1.8% and 4.7%. The within-subject coefficient of variance for the white-matter shear-stiffness measurement was 3.7% at 60 Hz.

Table 1
Mean shear modulus of white matter, gray matter, and whole brains for all subjects at all three frequencies.

	60 Hz	50 Hz	40 Hz
μ White Matter [kPa]	3.85 ± 0.12	3.78 ± 0.15	3.36 ± 0.11
μ Gray Matter [kPa]	3.33 ± 0.14	2.82 ± 0.16	2.24 ± 0.14
μ Whole Brain [kPa]	3.27 ± 0.05	3.04 ± 0.05	2.57 ± 0.04

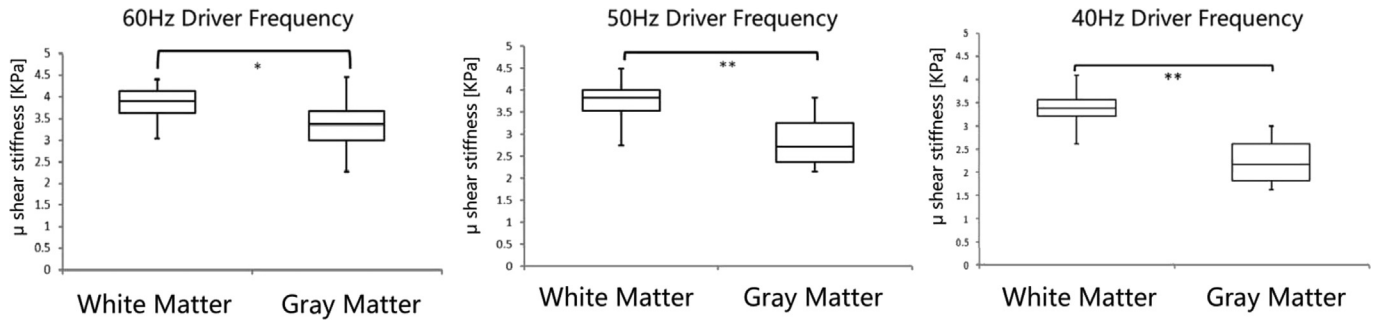

Fig. 5. Boxplots displaying the full range of variation (from minimum to maximum) of shear stiffness for white matter and gray matter within the specified ROIs at frequencies of 60 Hz, 50 Hz, and 40 Hz.
* Denotes a pairwise statistically significant difference between white matter and gray matter, with a P value of < 0.05, while ** denotes a pairwise statistically significant difference between white matter and gray matter, with a P value of < 0.001.

Table 2
Analysis of variance results for white matter, gray matter, and whole brain (SS, the sum of squares due to the source; MS, the mean sum of squares due to the source; F, the found variation of the group averages; and F critical, the expected variation of the group averages).

Source of variation	SS	df	MS	F	P-value	F critical
Frequency in white matter	2.03	2	1.02	17.54	$P < 0.001$	3.55
Frequency in gray matter	6.26	2	3.13	51.58	$P < 0.001$	3.55
Frequency in whole brain	2.59	2	1.29	283.92	$P < 0.001$	3.55

4. Discussion

In this study, an ergonomically flexible driver was designed to allow mechanical waves to be effectively induced into the brain while occupying a minimum volume in an MRI head coil for MRE examination. A 2D finite-element simulation and waveform images of all subjects indicate that shear waves can be effectively propagated thoroughly into the whole brain. No volunteers in this study complained about any discomfort.

Brain MRE scans require a driver that can generate and propagate waves to the brain, which must be as close as possible to the surface of the scanned target to spread mechanical excitation to the target tissue [2,31,33,34]. Following an actuator design, the subject placed his or her head on a cradle, which was attached to an actuator at the end of the patient's table [35]. The actuator cradle was placed inside the head coil. The driving device is complicated in structure, inconvenient to use, and sometimes produces artifacts in the posterior region of the skull. Several studies on MRE of the head use cradle-like passive actuators [19,20,33,36]. When using a bite stick, the subject bites a thermoplastic block attached to the actuator with his or her teeth, which mechanically actuates the head [13]. The diversity of these drivers for generating vibrational waves indicates the lack of a standard MRE driver design for determining the stiffness of brain tissue. In order for MRE to serve as a quantitative imaging biomedical marker, standardization of driver design and MRE protocol is imperative. An assessment of reliability is crucial for clinical MRE examinations [37].

In this study, we designed the shape of the pillow-shaped actuator and redesigned it in a round shape that makes it easier to fit into the head coil. We added a solid, flexible internal structure so the air could better fill the drive in its uninflated state, and we also added a skin marker to ensure that the driver could be placed in the appropriate vibration location. The whole-brain shear stiffness at 60 Hz was 3.27 ± 0.16 kPa, which is similar to the results of a whole-brain shear-stiffness test using a rectangular pillow driver at 60 Hz (3.01 kPa) [14]. When the frequency is 50 Hz, the shear stiffness of the gray matter component measured by Johnson et al. is between about 3–4 kPa. It is higher than our measurement at 50 Hz (2.82 ± 0.16 kPa). The reason for this phenomenon may be that the inversion algorithm is different. We use the Helmholtz inversion algorithm, and Johnson et al. use the nonlinear inversion.

A one-way analysis of variance indicated that shear-stiffness measurements in the brain are frequency-dependent. The shear stiffness seems to increase with driver frequency. When higher driving

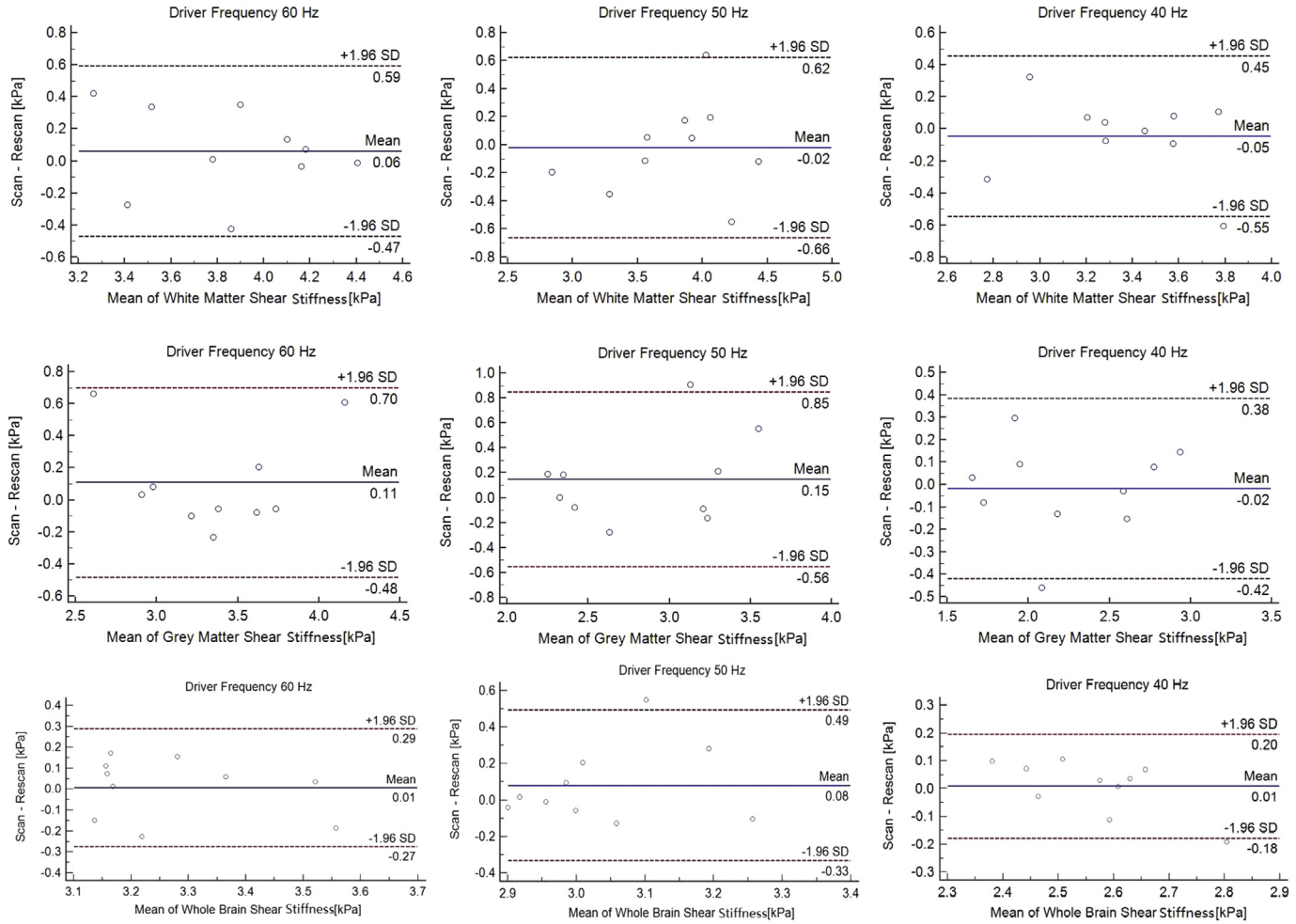

Fig. 6. A Bland-Altman plot of the difference between the scan and rescan for white-matter, gray-matter, and whole-brain shear-stiffness measurements, where each dot represents a patient's measurement.

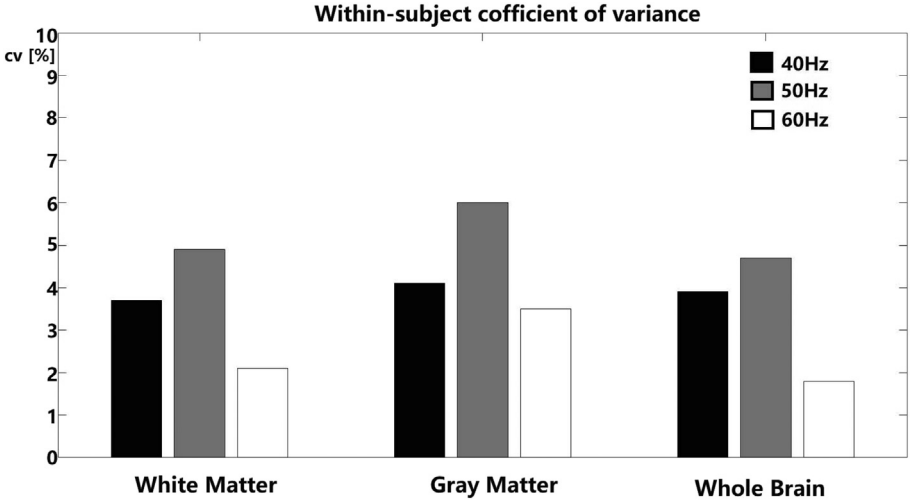

Fig. 7. The within-subject coefficients of variance at driver frequencies of 60, 50, and 40 Hz.

frequencies are used, brain tissue shows higher stiffness on the MRE. The results of Sack et al. show that as the frequency increases from 25 Hz to 62.5 Hz, the storage and loss moduli increases with growing frequency [35,38]. Higher frequencies with shorter wavelengths increase the resolution of the MRE image, but the accompanying attenuation of the signal increases proportionally, which reduces the signal-to-noise ratio [3]. Likewise, lower frequencies and longer wavelengths may cause a loss of spatial resolution and may limit the ability to detect small tumors [10]. Due to this contradiction, the single optimal mechanical frequency of brain MRE imaging is crucial for the standardization of MRE measurement.

A significant statistical difference was found between white and gray matter. One study used indentation to determine the shear stiffness of white and gray matter in cows' ex vivo brains to be 1.895 and 1.389 kPa, respectively [39]. Mechanical tests by Xu et al. on adult ex vivo ferrets showed that white matter is harder than gray at low strain rates [40]. The human brain has similar properties to the animal brain. Its shear stiffness was found to be higher in white matter than in gray matter [13,41–43]. This finding seems to align with the general consensus that white matter is stiffer due to the fiber tracts present in it.

After completion of the first scan, the subjects left the bed themselves and then returned to it and were rescanned using exactly the same procedure. All Bland-Altman plots showed good reproducibility at all frequencies. The within-subject coefficient of variance was below 6% for white matter, gray matter, and the whole brain, which shows that shear stiffness serves as a highly reproducible imaging biomarker. Another study by Johnson et al. showed that the CV for each measurement of gray matter and white matter was < 10%, indicating excellent reproducibility of the MRE results [36]. In the experiment that measured the hardness of the brain region, the repeatability of the measurement results improved obviously after SNR calculation. For lobes, deep GM/WM- and cerebellar-region tests showed that the repetitive reliability was high, with median CV < 1.98% and maximum CV < 4.48% [44]. The CV of most components in the gray matter measured by Johnson et al. fell between 3% and 7%. The CV of the whole brain is very small (1.4%) because of its much larger volume [45]. Murphy et al. reported a coefficient of variance of < 3.1% for the whole brain [14]. Our study of the reproducibility of the whole brain modulus is based on MRE scans at different frequencies. The minimum and maximum values of the CV between the two scans were 1.8% and 3.5%, respectively. Testu et al. verified that it is feasible and reproducible to use the MRE scan to estimate the power-law behavior of viscoelasticity in the human brain [46].

This study has several limitations. First, the brain was scanned using a T2 weighted sequence for gray-matter and white-matter ROI placement. After consulting with experienced radiologists, we found that white matter in T1W images was easier to distinguish. In future study, T1-weighted sequences will be acquired for brain-tissue ROI placement. Second, the subject population included 10 healthy volunteers whose ages ranged from 24 to 38 years. This population was relatively young, so the scan results did not reflect changes in shear stiffness due to age, and there was no comparison of shear-stiffness differences between men and women. A larger group of subjects should be used in future studies, with a broader age span and a balance between males and females. Third, all volunteers were healthy subjects. Patients with brain diseases might be recruited for MRE scans to explore the effectiveness of the pneumatic drivers in detecting diseases. Fourth, a two-dimensional MRE scan was used and only the propagation of waves within the imaging plane were taken into consideration. Future research could use 3D MRE to generate elasticity maps for more accurate estimation [22,47]. The algorithm used to reconstruct the elasticity map assumed that the material was isotropic. In fact, material testing of animal brains shows that the mechanical anisotropy of brain tissue is significant, and human brains are expected to exhibit similar properties [48], so ignoring anisotropy could lead to underestimation or overestimation of shear stiffness in brain tissue. Romano et al. showed that brain tissue has slight anisotropy, while the white matter mass acts as a waveguide that propagates shear waves [49]. The anisotropic mechanical properties of biological tissues may be assessed with a combination of MRE and DTI [50]. Finally, the passive driver, head coil, and skin marker were separate from each other. It is necessary to integrate the driver and skin marker into the head coil in future designs to allow for a simple implementation of MRE protocol.

5. Conclusion

This study shows that a novel ergonomic pillow-like pneumatic passive driver for the brain can be used to efficiently measure the elastic modulus of white matter, gray matter, and the entire brain. MRE scanning of the head at 3 T has good repeatability and frequency correlation. The use of brain MRE technology as a quantitative imaging biomarker for brain-stiffness measurement requires further improvement, particularly within techniques such as frequency standardization, 3D acquisition, and the integration of the head coil with the passive driver.

Funding

This work was supported by the Xidian University and Free Exploration Fund of the Ministry of Education of China.

Acknowledgements

We would like to express our thanks to Dr. Mingqiu Luo and Dr. Changhua Zhang (BroadGeo Inc. Houston, TX) for their help on 2-dimensional finite-element simulation and discussions, and to Dr. Arunark Kolipaka (The Ohio state University) for his help on phase difference SNR (PDSNR) calculation and discussions.

References

[1] Manduca A, Oliphant TE, Dresner MA, Mahowald JL, Kruse SA, Amromin E, et al. Magnetic resonance elastography: non-invasive mapping of tissue elasticity. Med Image Anal 2001;5:237–54. https://doi.org/10.1016/S1361-8415(00)00039-6.

[2] Di Ieva A, Grizzi F, Rognone E, Tse ZTH, Parittotokkaporn T, Rodriguez Y, et al. Magnetic resonance elastography: a general overview of its current and future applications in brain imaging. Neurosurg Rev 2010;33:137–45. discussion 145 https://doi.org/10.1007/s10143-010-0249-6.

[3] Chartrain AG, Kurt M, Yao A, Feng R, Nael K, Mocco J, et al. Utility of preoperative meningioma consistency measurement with magnetic resonance elastography (MRE): a review. Neurosurg Rev 2017. https://doi.org/10.1007/s10143-017-0862-8.

[4] Muthupillai R, Lomas DJ, Rossman PJ, Greenleaf JF, Manduca A, Ehman RL. Magnetic resonance elastography by direct visualization of propagating acoustic strain waves. Science 1995;269:1854–7.

[5] Okamoto RJ, Clayton EH, Bayly PV. Viscoelastic properties of soft gels: comparison of magnetic resonance elastography and dynamic shear testing in the shear wave regime. Phys Med Biol 2011;56:6379–400. https://doi.org/10.1088/0031-9155/56/19/014.

[6] Hiscox LV, Johnson CL, Barnhill E, McGarry MDJ, Huston J, van Beek EJR, et al. Magnetic resonance elastography (MRE) of the human brain: technique, findings and clinical applications. Phys Med Biol 2016;61:R401–37. https://doi.org/10.1088/0031-9155/61/24/R401.

[7] Yin M, Talwalkar JA, Glaser KJ, Manduca A, Grimm RC, Rossman PJ, et al. Assessment of hepatic fibrosis with magnetic resonance elastography. Clin Gastroenterol Hepatol 2007;5:1207–1213.e2. https://doi.org/10.1016/j.cgh.2007.06.012.

[8] Kolipaka A, Wassenaar PA, Cha S, Marashdeh WM, Mo X, Kalra P, et al. Magnetic resonance elastography to estimate brain stiffness: measurement reproducibility and its estimate in pseudotumor cerebri patients. Clin Imaging 2018;51:114–22. https://doi.org/10.1016/j.clinimag.2018.02.005.

[9] Zhang J, Green MA, Sinkus R, Bilston LE. Viscoelastic properties of human cerebellum using magnetic resonance elastography. J Biomech 2011;44:1909–13. https://doi.org/10.1016/j.jbiomech.2011.04.034.

[10] Hawley JR, Kalra P, Mo X, Raterman B, Yee LD, Kolipaka A. Quantification of breast stiffness using MR elastography at 3 Tesla with a soft sternal driver: a reproducibility study. J Magn Reson Imaging 2017;45:1379–84. https://doi.org/10.1002/jmri.25511.

[11] Sinkus R, Tanter M, Xydeas T, Catheline S, Bercoff J, Fink M. Viscoelastic shear properties of in vivo breast lesions measured by MR elastography. Magn Reson Imaging 2005;23:159–65. https://doi.org/10.1016/j.mri.2004.11.060.

[12] Arani A, Plewes D, Krieger A, Chopra R. The feasibility of endorectal MR elastography for prostate cancer localization. Magn Reson Med 2011;66:1649–57. https://doi.org/10.1002/mrm.22967.

[13] Xu L, Lin Y, Han JC, Xi ZN, Shen H, Gao PY. Magnetic resonance elastography of brain tumors: preliminary results. Acta radiologica (Stockholm, Sweden: 1987) 2007;48:327–30. https://doi.org/10.1080/02841850701199967.

[14] Murphy MC, Huston J, Jack CR, Glaser KJ, Manduca A, Felmlee JP, et al. Decreased brain stiffness in Alzheimer's disease determined by magnetic resonance elastography. J Magn Reson Imaging 2011;34:494–8. https://doi.org/10.1002/jmri.22707.

[15] ElSheikh M, Arani A, Perry A, Boeve BF, Meyer FB, Savica R, et al. MR elastography demonstrates unique regional brain stiffness patterns in dementias. AJR Am J Roentgenol 2017;209:403–8. https://doi.org/10.2214/AJR.16.17455.

[16] Olivero WC, Wszalek T, Wang H, Farahvar A, Rieth SM, Johnson CL. Magnetic resonance elastography demonstrating low brain stiffness in a patient with low-pressure hydrocephalus: case report. Pediatr Neurosurg 2016;51:257–62. https://doi.org/10.1159/000445900.

[17] Perry A, Graffeo CS, Fattahi N, ElSheikh MM, Cray N, Arani A, et al. Clinical correlation of abnormal findings on magnetic resonance elastography in idiopathic normal pressure hydrocephalus. World Neurosurg 2017;99:695–700.e1. https://doi.org/10.1016/j.wneu.2016.12.121.

[18] Riek K, Millward JM, Hamann I, Mueller S, Pfueller CF, Paul F, et al. Magnetic resonance elastography reveals altered brain viscoelasticity in experimental autoimmune encephalomyelitis. NeuroImage Clinical 2012;1:81–90. https://doi.org/10.1016/j.nicl.2012.09.003.

[19] Streitberger K-J, Sack I, Krefting D, Pfüller C, Braun J, Paul F, et al. Brain viscoelasticity alteration in chronic-progressive multiple sclerosis. PLoS One 2012;7:e29888https://doi.org/10.1371/journal.pone.0029888.

[20] Fehlner A, Behrens JR, Streitberger K-J, Papazoglou S, Braun J, Bellmann-Strobl J, et al. Higher-resolution MR elastography reveals early mechanical signatures of neuroinflammation in patients with clinically isolated syndrome. J Magn Reson Imaging 2016;44:51–8. https://doi.org/10.1002/jmri.25129.

[21] Johnson CL, Telzer EH. Magnetic resonance elastography for examining developmental changes in the mechanical properties of the brain. Dev Cogn Neurosci 2017. https://doi.org/10.1016/j.dcn.2017.08.010.

[22] Pattison AJ, Lollis SS, Perriñez PR, Perreard IM, McGarry MDJ, Weaver JB, et al. Time-harmonic magnetic resonance elastography of the normal feline brain. J Biomech 2010;43:2747–52. https://doi.org/10.1016/j.jbiomech.2010.06.008.

[23] Yeung DKW, Bhatia KS, Lee YYP, King AD, Garteiser P, Sinkus R, et al. MR elastography of the head and neck: driver design and initial results. Magn Reson Imaging 2013;31:624–9. https://doi.org/10.1016/j.mri.2012.09.008.

[24] Latta P, Gruwel ML, Debergue P, Matwiy B, Sboto-Frankenstein UN, Tomanek B. Convertible pneumatic actuator for magnetic resonance elastography of the brain. Magn Reson Imaging 2011;29:147–52. https://doi.org/10.1016/j.mri.2010.07.014.

[25] Murphy MC, Jones DT, Jack CR, Glaser KJ, Senjem ML, Manduca A, et al. Regional brain stiffness changes across the Alzheimer's disease spectrum. NeuroImage Clinical 2016;10:283–90. https://doi.org/10.1016/j.nicl.2015.12.007.

[26] Huston J. Magnetic resonance elastography of the brain. In: Venkatesh SK, editor. Magnetic resonance elastography New York: Springer; 2014. p. 89–98. https://doi.org/10.1007/978-1-4939-1575-0_8.

[27] Geuzaine Christophe, Remacle Jean-Francois. Gmsh: a three-dimensional finite element mesh generator with built-in pre- and post-processing facilities. 0. 2009. p. 1–24.

[28] Komatitsch D, Erlebacher G, Göddeke D, Michéa D. High-order finite-element seismic wave propagation modeling with MPI on a large GPU cluster. J Comput Phys 2010;229:7692–714. https://doi.org/10.1016/j.jcp.2010.06.024.

[29] Oliphant TE, Manduca A, Ehman RL, Greenleaf JF. Complex-valued stiffness reconstruction for magnetic resonance elastography by algebraic inversion of the differential equation. Magn Reson Med 2001;45:299–310. https://doi.org/10.1002/1522-2594(200102)45:2<299:AID-MRM1039>3.0.CO;2-O.

[30] Murphy MC, Glaser KJ, Manduca A, Felmlee JP, Huston J, Ehman RL. Analysis of time reduction methods for magnetic resonance elastography of the brain. Magn Reson Imaging 2010;28:1514–24. https://doi.org/10.1016/j.mri.2010.06.016.

[31] Petrov AY, Sellier M, Docherty PD, Chase JG. Parametric-based brain Magnetic Resonance Elastography using a Rayleigh damping material model. Comput Methods Programs Biomed 2014;116:328–39. https://doi.org/10.1016/j.cmpb.2014.05.006.

[32] Martin Bland J, Altman D. Statistical methods for assessing agreement between two methods of clinical measurement. The Lancet 1986;327:307–10. https://doi.org/10.1016/S0140-6736(86)90837-8.

[33] Wuerfel J, Paul F, Beierbach B, Hamhaber U, Klatt D, Papazoglou S, et al. MR-elastography reveals degradation of tissue integrity in multiple sclerosis. NeuroImage 2010;49:2520–5. https://doi.org/10.1016/j.neuroimage.2009.06.018.

[34] Guo J, Hirsch S, Fehlner A, Papazoglou S, Scheel M, Braun J, Sack I. Towards an elastographic atlas of brain anatomy. PloS one 2013;8:e71807. https://doi.org/10.1371/journal.pone.0071807.

[35] Sack I, Beierbach B, Wuerfel J, Klatt D, Hamhaber U, Papazoglou S, et al. The impact of aging and gender on brain viscoelasticity. NeuroImage 2009;46:652–7. https://doi.org/10.1016/j.neuroimage.2009.02.040.

[36] Johnson CL, McGarry MDJ, Gharibans AA, Weaver JB, Paulsen KD, Wang H, et al. Local mechanical properties of white matter structures in the human brain. NeuroImage 2013;79:145–52. https://doi.org/10.1016/j.neuroimage.2013.04.089.

[37] Jia G, Heymsfield SB, Zhou J, Yang G, Takayama Y. Quantitative biomedical imaging: techniques and clinical applications. Biomed Res Int 2016;2016:3080965. https://doi.org/10.1155/2016/3080965.

[38] Sack I, Streitberger K-J, Krefting D, Paul F, Braun J. The influence of physiological aging and atrophy on brain viscoelastic properties in humans. PLoS One 2011;6:e23451https://doi.org/10.1371/journal.pone.0023451.

[39] Budday S, Nay R, de Rooij R, Steinmann P, Wyrobek T, Ovaert TC, et al. Mechanical properties of gray and white matter brain tissue by indentation. J Mech Behav Biomed Mater 2015;46:318–30. https://doi.org/10.1016/j.jmbbm.2015.02.024.

[40] Xu G, Knutsen AK, Dikranian K, Kroenke CD, Bayly PV, Taber LA. Axons pull on the brain, but tension does not drive cortical folding. J Biomech Eng 2010;132:71013. https://doi.org/10.1115/1.4001683.

[41] Clayton EH, Genin GM, Bayly PV. Transmission, attenuation and reflection of shear waves in the human brain. J R Soc Interface 2012;9:2899–910. https://doi.org/10.1098/rsif.2012.0325.

[42] Kruse SA, Rose GH, Glaser KJ, Manduca A, Felmlee JP, Jack CR, et al. Magnetic resonance elastography of the brain. NeuroImage 2008;39:231–7. https://doi.org/10.1016/j.neuroimage.2007.08.030.

[43] McCracken PJ, Manduca A, Felmlee J, Ehman RL. Mechanical transient-based magnetic resonance elastography. Magn Reson Med 2005;53:628–39. https://doi.org/10.1002/mrm.20388.

[44] Murphy MC, Huston J, Jack CR, Glaser KJ, Senjem ML, Chen J, et al. Measuring the characteristic topography of brain stiffness with magnetic resonance elastography. PLoS One 2013;8:e81668https://doi.org/10.1371/journal.pone.0081668.

[45] Johnson CL, Schwarb H, D J McGarry M, Anderson AT, Huesmann GR, Sutton BP, et al. Viscoelasticity of subcortical gray matter structures. Hum Brain Mapp 2016;37:4221–33. https://doi.org/10.1002/hbm.23314.

[46] Testu J, McGarry MDJ, Dittmann F, Weaver JB, Paulsen KD, Sack I, et al. Viscoelastic power law parameters of in vivo human brain estimated by MR elastography. J Mech Behav Biomed Mater 2017;74:333–41. https://doi.org/10.1016/j.jmbbm.2017.06.027.

[47] Feng Y, Clayton EH, Chang Y, Okamoto RJ, Bayly PV. Viscoelastic properties of the ferret brain measured in vivo at multiple frequencies by magnetic resonance elastography. J Biomech 2013;46:863–70. https://doi.org/10.1016/j.jbiomech.2012.12.024.

[48] Anderson AT, van Houten EEW, McGarry MDJ, Paulsen KD, Holtrop JL, Sutton BP, et al. Observation of direction-dependent mechanical properties in the human brain

with multi-excitation MR elastography. J Mech Behav Biomed Mater 2016;59:538–46. https://doi.org/10.1016/j.jmbbm.2016.03.005.
[49] Romano A, Scheel M, Hirsch S, Braun J, Sack I. In vivo waveguide elastography of white matter tracts in the human brain. Magn Reson Med 2012;68:1410–22. https://doi.org/10.1002/mrm.24141.
[50] Qin EC, Sinkus R, Geng G, Cheng S, Green M, Rae CD, et al. Combining MR elastography and diffusion tensor imaging for the assessment of anisotropic mechanical properties: a phantom study. J Magn Reson Imaging 2013;37:217–26. https://doi.org/10.1002/jmri.23797.